Higher period ordered phases on the Bethe lattice

Ch. Gruber,[1] N. Macris,[1] Ph. Royer,[1] and J. K. Freericks[2]
[1]*Institut de Physique Théorique, École Polytechnique Fédérale de Lausanne, CH-1015, Lausanne, Switzerland*
[2]*Department of Physics, Georgetown University, Washington, DC 20057*
(Received 27 October 2000; published 4 April 2001)

We solve for period-three ordered phases on the infinite-coordination Bethe lattice. The model we have chosen to analyze is the spinless Falicov-Kimball model (although we believe these results should have more general validity). Contrary to the belief of many researchers in the field, the Bethe lattice can support higher period ordered phases even though there is no ''momentum space'' associated with the lattice. These higher period phases can be rigorously shown to appear at zero temperature and a numerical analysis indicates that their thermodynamic phase transition from the homogeneous, period-two, or higher period ordered phases is generically a first-order transition.

DOI: 10.1103/PhysRevB.63.165111 PACS number(s): 71.10.Fd, 71.10.Hf

I. INTRODUCTION

Phase diagrams of quantum statistical models are much less understood than their classical counterparts. This is because the quantum fluctuations make both low-temperature and ground-state properties difficult to determine. During the last decade, starting with the work of Metzner and Vollhardt,[1] progress has been made in the limit of infinite dimensions. As in classical statistical mechanics, it turns out that, in this limit, the lattice problem has a mean-field character, with the order parameter being self-consistently related to a local mean field. The self-consistent equations generally correspond to an effective single-site (or few-sites) system that represents a significant simplification with respect to the original problem. However, an important difficulty related to quantum fluctuations is that these equations remain dynamical (or more precisely, frequency dependent) and are therefore difficult to solve. As a consequence, in practice, one can compare only a limited number of broken-symmetry candidate phases and it is possible to miss the true ground-state and low-temperature behavior. A thorough review of these methods in the field of strongly correlated electronic models has already appeared.[2]

In this paper we examine the infinite-dimensional limit for a simple model that has both quantum and classical degrees of freedom, namely the Falicov-Kimball model.[3] It is defined on a finite lattice Λ consisting of a set of sites x and bonds $\{x,y\}$. Spinless fermions have a kinetic energy given by a hopping matrix $t_{xy}=t$ if $\{x,y\}$ is a bond of Λ and $t_{xy}=0$ otherwise. There is an on-site interaction between itinerant fermions and static particles (ions) whose configurations are defined by the occupation numbers $w_x=0,1$ for $x\in\Lambda$. In terms of creation and annihilation operators $c_x^\dagger$, c_x of fermions, the Hamiltonian is

$$H(\{w_x\})=-\sum_{x,y\in\Lambda} t_{xy}c_x^\dagger c_y+U\sum_{x\in\Lambda} w_x c_x^\dagger c_x, \qquad (1)$$

for a given configuration $\{w_x\}$ of ions. This model was introduced in 1969 by Falicov and Kimball[3] to study metal-insulator transitions in mixed-valence compounds of rare earth and transition-metal oxides. For such systems the classical variables w_x describe localized f electrons and the spinless fermions are the itinerant d electrons. Later, the model has been considered to study ordering in mixed-valence systems,[4] order-disorder transitions in binary alloys,[5] and itinerant magnetism.[6] It was reinvented by Kennedy and Lieb[6] as a primitive model of matter to study the origin of crystalline order. In their interpretation, classical particles represent ions and the quantum particles are the itinerant electrons ($U<0$ corresponds to the attraction between electrons and ions). We adopt this last interpretation here. Despite the simplicity of the Hamiltonian, the Falicov-Kimball model has been the object of many investigations and turns out to have a rich phase diagram. We refer the interested reader to the recent reviews.[7]

The Falicov-Kimball model has been extensively studied in one and two dimensions for large coupling U[8–10] and in one dimension for small U.[11,9,12] Here, we briefly summarize the situation for the periodic ground states that appear for large U, since this is the subject of the present investigation when the dimension is infinite. We define the electron density to be $\rho_e=\Sigma_x\langle c_x^\dagger c_x\rangle/|\Lambda|$ and the ion density to be $\rho_i=\Sigma_x w_x/|\Lambda|$ with $|\Lambda|$ the number of lattice sites in the lattice Λ. In one dimension, for rational densities $\rho_e=\rho_i=p/q$ (p,q relatively prime integers) the ground states have period q, with p ions arranged in the ''most homogeneous way'' within each period for $U>U_c(q)$.[8] As a function of chemical potential, the ground states are organized according to a Farey tree structure.[13] We stress that it is still an open problem to determine if the complete Farey tree appears for finite U, i.e., if one can find U_c independent of q. In two dimensions, periodic ground states are known to exist[15,14,10] for U large and densities $\frac{1}{2}$, $\frac{1}{3}$, $\frac{1}{4}$, $\frac{1}{5}$, and $\frac{2}{9}$. Surprisingly, however, for rational densities in the open intervals $]\frac{1}{5},\frac{2}{9}[$ and $]\frac{2}{9},\frac{1}{4}[$ the ground state is a mixture of periodic states.[16] This phase separation can be traced back to frustration effects present on the two-dimensional square lattice.[16,17]

In the limit of infinite dimension, Brandt and Mielsch[18] computed exactly the staggered susceptibility for the hypercubic lattice and were able to find the transition temperature T_c between the high-temperature disordered phase and a low-temperature ordered chessboard phase. They found that

T_c behaves as $1/U$ for $U\to\infty$ and $U^2 \ln U^{-1}$ for $U\to 0$, and that the transition is second-order Ising-like. Freericks has studied incommensurate and segregated phases on the hypercubic lattice,[19] and more recently, we have studied[20] phase separation on the Bethe and hypercubic lattices for infinite coupling strength $U=\infty$ and for finite[21] U.

In the present contribution, we address the question of the existence of general periodic crystalline ground states, in the limit of infinite dimension, for periods that are greater than two. We have developed a formalism to investigate the problem when Λ is a Bethe lattice of infinite coordination number. We prove that besides the period-two chessboard phase studied previously by many authors, there exist higher period phases (most likely period-three) at $T=0$. Our study suggests that even higher periods also exist, much like those in one dimension. We also show that the period-three phase is stable for low temperatures but has a generically first-order phase transition to higher period phases as a function of temperature. At this point, we wish to stress that it is not obvious that the Bethe lattice with an infinite coordination number is equivalent to the hypercubic lattice $\mathbf{Z}^d$ with $d\to\infty$ (especially for the higher period phases). For example, while it is clear how to define the susceptibility for a general wave vector k in $\mathbf{Z}^d$, we have not succeeded in doing so for higher period phases on the Bethe lattice except for the already known uniform and staggered cases (if indeed the transition is actually first order, then this exercise yields no useful information anyway). Furthermore, loops in the hypercubic lattice may introduce frustration effects that can destroy crystalline order (recall the two-dimensional case[15]) that are not present on the Bethe lattice. The main reasons we have chosen to study the Bethe lattice is that the self-consistent equations are more tractable and we are able to resolve this controversy about the existence of higher period phases.

Specifically, for Λ we take a tree of coordination number Z and perform the scaling $t_{xy}\to t_{xy}^*/\sqrt{Z}$ in Eq. (1). Under some reasonable assumptions, we obtain an exact set of equations describing period-q states in the limit when $|\Lambda|\to\infty$ and $Z\to\infty$. The picture that we have in mind for the period-q configurations is as follows. One selects a special site 0 (the level zero site or the root of the tree) connected to Z level 1 sites, which are in turn connected to $Z(Z-1)$ level 2 sites and so on. The ion configurations that we find are ordered periodically along the levels of the tree. In the limit $Z\to\infty$, we find regions of phase space where the segregated, homogeneous, and period-two phases are not the ground state, because a restricted phase diagram shows regions where period-three phases are stabilized, organized qualitatively in the same way as in the one- or two-dimensional cases. Crystalline states of ion density other than $\frac{1}{2}$ therefore exist on the Bethe lattice, a fact that had not been established previously (and in fact has been assumed by many not to occur).

The paper is organized as follows. In Sec. II we give a derivation of the self-consistent equations for the period-q states when $Z\to\infty$. Our equations are exact and valid for any coupling strength U and inverse temperature β. In Sec. III we formulate the ground-state problem by deriving a set of limiting equations when $\beta\to\infty$ that are valid for all U. Section IV contains a numerical study of the finite-temperature equations for moderate values of U and shows the existence of higher period phases at low temperatures. Finally, we conclude with open questions that could be investigated within the present formalism in Sec. V.

II. FORMALISM ON THE BETHE LATTICE

In this section we derive the exact equations satisfied by the Green functions in the limit of an infinite coordination number for a Bethe lattice. We begin by considering a finite tree Λ with coordination number Z and rescale the hopping term in the Hamiltonian in Eq. (1) as $t_{xy}\to t_{xy}^*/\sqrt{Z}$. The imaginary time Green function is defined for $\tau>0$ and $y,z\in\Lambda$ as

$$G_{yz}^{\Lambda}(\tau)=-\frac{1}{Z_\Lambda}\sum_{\{w_x=0,1\}} e^{\beta\mu_i N_i}\mathrm{Tr}\, c_y(\tau)c_z^\dagger(0) \times e^{-\beta[H(\{w_x\})-\mu_e N_e]}, \tag{2}$$

where $N_i=\Sigma_{x\in\Lambda}w_x$ is the total ion number, $N_e=\Sigma_{x\in\Lambda}c_x^\dagger c_x$ the total electron number, and μ_i,μ_e are their respective chemical potentials. In Eq. (2),

$$c_y(\tau)=e^{\tau[H(\{w_x\})-\mu_e N_e]}c_y e^{-\tau(H[\{w_x\})-\mu_e N_e]}. \tag{3}$$

It is convenient to use Grassmann variables $\overline{\psi}_x(\tau)$, $\psi_x(\tau)$, $x\in\Lambda$, $\tau\in[0,\beta]$ to describe the electronic degrees of freedom. The Green function in Eq. (2) can be represented by the functional integral

$$\begin{aligned} G_{yz}^{\Lambda}(\tau)&=-\langle\psi_y(\tau)\overline{\psi}_z(0)\rangle_\Lambda \\ &=-\frac{1}{Z_\Lambda}\sum_{\{w_x=0,1\}} e^{\beta\mu_i N_i} \\ &\quad\times\int D\overline{\psi}D\psi\psi_y(\tau)\overline{\psi}_z(0)e^{-S^\Lambda(\{w_x\})}, \end{aligned} \tag{4}$$

where $S^\Lambda(\{w_x\})$ is the action corresponding to the Hamiltonian in Eq. (1)

$$S^\Lambda(\{w_x\})=\sum_{y,z\in\Lambda}\int_0^\beta d\tau'\,\overline{\psi}_y(\tau') \times\left[\delta_{yz}\frac{\partial}{\partial\tau'}-\frac{t_{yz}^*}{\sqrt{Z}}+\delta_{yz}(Uw_y-\mu_e)\right]\psi_z(\tau'). \tag{5}$$

Since the Grassmann variables satisfy antiperiodic boundary conditions $\psi_y(\beta)=-\psi_y(0)$ and $\overline{\psi}_y(\beta)=-\overline{\psi}_y(0)$, their Fourier modes $\overline{\psi}_y(i\omega_n),\psi_y(i\omega_n)$ are defined by

$$\psi_y(\tau)=\sum_{n=-\infty}^{\infty}\frac{e^{-i\omega_n\tau}}{\sqrt{\beta}}\psi_y(i\omega_n),$$

$$\overline{\psi}_y(\tau)=\sum_{n=-\infty}^{\infty}\frac{e^{i\omega_n\tau}}{\sqrt{\beta}}\overline{\psi}_y(i\omega_n), \tag{6}$$

with $\omega_n=(2n+1)\pi\beta^{-1}$ the Matsubara frequencies. In terms of this new set of Grassmann variables, the action in Eq. (5) becomes

$$S^{\Lambda}(\{w_x\})=\sum_{n=-\infty}^{\infty}S_n^{\Lambda}(\{w_x\}), \tag{7}$$

where

$$S_n^{\Lambda}(\{w_x\})=\sum_{y,z\in\Lambda}\left[(-i\omega_n-\mu_e+Uw_y)\delta_{yz}-\frac{t_{yz}^*}{\sqrt{Z}}\right]\times\overline{\psi}_y(i\omega_n)\psi_z(i\omega_n). \tag{8}$$

Our basic quantity of interest is the nth Fourier mode of the local Green function

$$G_{yy}^{\Lambda}(i\omega_n)=-\langle\psi_y(i\omega_n)\overline{\psi}_y(i\omega_n)\rangle_{\Lambda}, \tag{9}$$

where the average is the same as in Eq. (2).

The first step in establishing the equations for the infinite-dimensional limit is to express the local Green function $G_{yy}^{\Lambda}(i\omega_n)$ in terms of the Green function associated with the lattice $\Lambda(y)$ obtained from Λ by removing the site y. Given y, the nth Fourier component of the action $S_n^{\Lambda}(\{w_x\})$ can be written in terms of the action $S_n^{\Lambda(y)}(\{w_x\})$ associated with $\Lambda(y)$ and a local piece associated to the site y

$$S_n^y=(-i\omega_n-\mu_e+Uw_y)\overline{\psi}_y(i\omega_n)\psi_y(i\omega_n), \tag{10}$$

as

$$S_n^{\Lambda}(\{w_x\})=S_n^{\Lambda(y)}(\{w_x\})+S_n^y-\sum_{z\in\Lambda,t_{yz}^*\neq 0}\frac{t_{yz}^*}{\sqrt{Z}}[\overline{\psi}_y(i\omega_n)\psi_z(i\omega_n)+\overline{\psi}_z(i\omega_n)\psi_y(i\omega_n)]. \tag{11}$$

Let $Z_{\Lambda(y)}$ and $\langle-\rangle_{\Lambda(y)}$ be the partition function and the average corresponding to $S_n^{\Lambda(y)}(\{w_x\})$. We have

$$G_{yy}^{\Lambda}(i\omega_n)=-\frac{Z_{\Lambda(y)}}{Z_{\Lambda}}\sum_{w_y=0,1}e^{\beta\mu_i w_y}\times\int D\overline{\psi}_yD\psi_y\psi_y(i\omega_n)\overline{\psi}_y(i\omega_n)e^{-S_n^y}\times\left\langle\exp\left\{\sum_{n=-\infty}^{\infty}\sum_{z,t_{yz}^*\neq 0}\frac{t_{yz}^*}{\sqrt{Z}}[\overline{\psi}_y(i\omega_n)\psi_z(i\omega_n)+\overline{\psi}_z(i\omega_n)\psi_y(i\omega_n)]\right\}\right\rangle_{\Lambda(y)}. \tag{12}$$

Since Λ is a tree of coordination number Z, $\Lambda(y)$ is the union of Z disjoint trees $\Lambda(y;z)$ associated to each z such that $t_{yz}^*\neq 0$. We note that for $\Lambda(y;z)$ the site z has coordination number $Z-1$ while all other sites have coordination number Z. The disjointness of the trees $\Lambda(y;z)$ implies

$$\left\langle\exp\left\{\sum_{n=-\infty}^{\infty}\sum_{z,t_{yz}^*\neq 0}\frac{t_{yz}^*}{\sqrt{Z}}[\overline{\psi}_y(i\omega_n)\psi_z(i\omega_n)+\overline{\psi}_z(i\omega_n)\psi_y(i\omega_n)]\right\}\right\rangle_{\Lambda(y)}=\prod_{z,t_{yz}^*\neq 0}\left\langle\exp\left\{\sum_{n=-\infty}^{\infty}\frac{t_{yz}^*}{\sqrt{Z}}[\overline{\psi}_y(i\omega_n)\psi_z(i\omega_n)+\overline{\psi}_z(i\omega_n)\psi_y(i\omega_n)]\right\}\right\rangle_{\Lambda(y;z)}. \tag{13}$$

Each average in the product is in fact a Gaussian integral so that only the second moment is needed

$$\tfrac{1}{2}\langle[\overline{\psi}_y(i\omega_n)\psi_z(i\omega_n)+\overline{\psi}_z(i\omega_n)\psi_y(i\omega_n)][\overline{\psi}_y(i\omega_m)\psi_z(i\omega_m)+\overline{\psi}_z(i\omega_m)\psi_y(i\omega_m)]\rangle_{\Lambda(y;z)}=-\overline{\psi}_y(i\omega_n)\psi_y(i\omega_n)G_{zz}^{\Lambda(y;z)}(i\omega_n)\delta_{nm}. \tag{14}$$

From Eqs. (12)–(14) we deduce

$$G_{yy}^{\Lambda}(i\omega_n)=-\frac{1}{Z_{\Lambda,eff}}\sum_{w_y=0,1}e^{\beta\mu_i w_y}\times\int D\overline{\psi}_yD\psi_y\psi_y(i\omega_n)\overline{\psi}_y(i\omega_n)e^{-\sum_{n=-\infty}^{\infty}S_{n,eff}^{\Lambda}(w_y)}, \tag{15}$$

with the local effective action associated with the single site y

$$S_{n,eff}^{\Lambda}(w_y)=\left[-i\omega_n-\mu_e+Uw_y+\frac{1}{Z}\sum_{z,t_{yz}^*\neq 0}t_{yz}^{*2}G_{zz}^{\Lambda(y;z)}(i\omega_n)\right]\overline{\psi}_y(i\omega_n)\psi_y(i\omega_n), \tag{16}$$

and the associated normalization factor

$$Z_{\Lambda,eff}=\frac{Z_{\Lambda}}{Z_{\Lambda(y)}}=\sum_{w_y=0,1}e^{\beta\mu_i w_y}\int D\overline{\psi}_yD\psi_ye^{-\sum_{n=-\infty}^{\infty}S_{n,eff}^{\Lambda}(w_y)}. \tag{17}$$

Proceeding in a similar way, one can derive expressions for the average number of ions at site y in terms of the local effective action in Eq. (16)

$$\langle w_y\rangle_{\Lambda}=\frac{e^{\beta\mu_i}}{Z_{\Lambda,eff}}\int D\overline{\psi}_yD\psi_ye^{-\sum_{n=-\infty}^{\infty}S_{n,eff}^{\Lambda}(1)}, \tag{18}$$

and

$$1-\langle w_y\rangle_\Lambda=\frac{1}{Z_{\Lambda,eff}}\int D\bar{\psi}_y D\psi_y e^{-\sum_{n=-\infty}^{\infty} S^\Lambda_{n,eff}(0)}. \quad (19)$$

Using Eqs. (18) and (19), the expression in Eq. (15) becomes

$$G^\Lambda_{yy}(i\omega_n)=-(1-\langle w_y\rangle_\Lambda)\langle\psi_y(i\omega_n)\bar{\psi}_y(i\omega_n)\rangle_0 - \langle w_y\rangle_\Lambda\langle\psi_y(i\omega_n)\bar{\psi}_y(i\omega_n)\rangle_1, \quad (20)$$

where the last two averages are with respect to $S^\Lambda_{n,eff}(0)$ and $S^\Lambda_{n,eff}(1)$, respectively. These are again Gaussian integrals that yield

$$G^\Lambda_{yy}(i\omega_n)=\frac{[1-\langle w_y\rangle_\Lambda]}{i\omega_n+\mu_e-\frac{1}{Z}\sum_z t^{*2}_{yz}G^{\Lambda(y;z)}_{zz}(i\omega_n)} + \frac{\langle w_y\rangle_\Lambda}{i\omega_n+\mu_e-U-\frac{1}{Z}\sum_z t^{*2}_{yz}G^{\Lambda(y;z)}_{zz}(i\omega_n)}. \quad (21)$$

From Eq. (18) we also find

$$\langle w_y\rangle_\Lambda=\left[1+e^{-\beta\mu_i}\prod_{n=-\infty}^{\infty}\frac{i\omega_n+\mu_e-\frac{1}{Z}\sum_z t^{*2}_{yz}G^{\Lambda(y;z)}_{zz}(i\omega_n)}{i\omega_n+\mu_e-U-\frac{1}{Z}\sum_z t^{*2}_{yz}G^{\Lambda(y;z)}_{zz}(i\omega_n)}\right]^{-1}. \quad (22)$$

Formulas (21) and (22) constitute an exact set of coupled equations for the local Green function for a finite lattice Λ with coordination number Z. We now proceed to take the thermodynamic limit and then the limit of an infinite-coordination number. These two steps are not done in a rigorous way and rely on some reasonable assumptions.

We assume that the thermodynamic limits of $G^\Lambda_{yy}(i\omega_n)$, $G^{\Lambda(y;z)}_{zz}(i\omega_n)$, and $\langle w_y\rangle_\Lambda$ exist and denote them, respectively, by $G_{yy}(i\omega_n)$, $G^*_{zz}(i\omega_n)$, and $\langle w_y\rangle$ (note the * superscript does not indicate complex conjugation here). Furthermore, we assume that the thermodynamic limit can be taken inside the infinite product appearing in Eq. (22), so that $\langle w_y\rangle$ is given by Eq. (22) with $G^{\Lambda(y;z)}_{yy}(i\omega_n)$ replaced by $G^*_{zz}(i\omega_n)$. These assumptions imply that the infinite-volume quantities satisfy Eqs. (21) and (22).

In order to take the infinite-coordination number limit, we first assume that in this limit the Green function $G^*_{zz}(i\omega_n)$, where the site z has coordination number $Z-1$, becomes equal to $G_{zz}(i\omega_n)$, where the site y has coordination number Z,

$$\lim_{Z\to\infty} G^*_{zz}(i\omega_n)=G_{zz}(i\omega_n). \quad (23)$$

In fact this assumption is justified to some extent in Appendix A where the first terms of an expansion of $G^{\Lambda(y;z)}_{zz}$ in powers of $1/Z$ are analyzed. From now on we set $x_0=0$ and call x_1 the Z sites of level 1, x_2 the $Z(Z-1)$ sites of level 2, and so forth. We assume that when $Z\to\infty$, for each integer q there exist limiting functions

$$\lim_{Z\to\infty} G_{x_j x_j}(i\omega_n)=g_j(i\omega_n), \quad j=0,1,\ldots,q-1, \quad (24)$$

and

$$\lim_{Z\to\infty}\langle w_{x_j}\rangle=\alpha_j, \quad j=0,1,\ldots,q-1, \quad (25)$$

describing period-q solutions. Using Eqs. (21) and (22) we see that the set of equations describing the period-q phases are

$$g_j(i\omega_n)=\frac{1-\alpha_j}{i\omega_n+\mu_e-t^{*2}g_{j+1}(i\omega_n)} + \frac{\alpha_j}{i\omega_n+\mu_e-U-t^{*2}g_{j+1}(i\omega_n)}, \quad (26)$$

with $g_q(i\omega_n)=g_0(i\omega_n)$ and

$$\alpha_j=\left[1+e^{-\beta\mu_i}\prod_{n=-\infty}^{\infty}\frac{i\omega_n+\mu_e-t^{*2}g_{j+1}(i\omega_n)}{i\omega_n+\mu_e-U-t^{*2}g_{j+1}(i\omega_n)}\right]^{-1}. \quad (27)$$

These equations are valid for finite temperatures and can only be solved by employing the numerical procedures discussed in Sec. IV. In the zero-temperature limit however, it is possible to develop a restricted-phase diagram analysis. This is the subject of the next section.

But before proceeding, we first want to remark that in the case $q=1$, our formalism becomes equivalent to the usual self-consistent method. In the later formulation, for an homogeneous phase, one has to solve a set of three-coupled equations.[2]

$$g_0(i\omega_n)=\int_{-2t^*}^{2t^*} d\epsilon\rho(\epsilon)\frac{1}{i\omega_n+\mu_e-\Sigma(i\omega_n)-\epsilon}, \quad (28)$$

with $\rho(\epsilon)=\sqrt{4t^{*2}-\epsilon^2}/2\pi t^{*2}$ the local noninteracting density of states and $\Sigma(i\omega_n)$ the local self-energy,

$$g_0(i\omega_n)=\frac{(1-\alpha_0)}{G_0^{-1}(i\omega_n)}+\frac{\alpha_0}{G_0^{-1}(i\omega_n)-U}, \tag{29}$$

and

$$G_0^{-1}(i\omega_n)=g_0^{-1}(i\omega_n)+\Sigma(i\omega_n), \tag{30}$$

where $G_0(i\omega_n)$ is called the effective medium and can be interpreted as the Green function with the local correlations removed. The algorithm for determining the homogeneous solution is to start with a trial self-energy and use Eq. (28) to determine the local Green function. The effective medium is then determined from Eq. (29), and a new trial self-energy is then found from Eq. (30). This loop is iterated until convergence is reached. In the present case, these equations can be reduced to Eq. (26) for $q=1$. Indeed, the integral can be done exactly and yields

$$g_0(i\omega_n)=\frac{i\omega_n+\mu_e-\Sigma(i\omega_n)}{2t^{*2}} -\frac{\sqrt{[i\omega_n+\mu_e-\Sigma(i\omega_n)]^2-4t^{*2}}}{2t^{*2}}, \tag{31}$$

(the branch of the square root is chosen to preserve the analyticity of g_0). Eliminating the self-energy between this equation and Eq. (30) we find

$$G_0^{-1}(i\omega_n)=i\omega_n+\mu_e-t^{*2}g_0(i\omega_n). \tag{32}$$

Finally, replacing this last expression in Eq. (29) gives Eq. (26) for $q=1$.

III. GROUND-STATE EQUATIONS

In the zero-temperature limit $\beta\to\infty$, the Matsubara frequencies $\omega_n=(2n+1)\pi\beta^{-1}$ form a continuum $\omega\in]-\infty,\infty[$ and as long as the chemical potentials are held fixed, Eq. (27) becomes

$$\alpha_j=\theta[X_j(\mu_e,\mu_i)], \tag{33}$$

where

$$X_j(\mu_e,\mu_i)=\mu_i-\int_{-\infty}^{\infty}\frac{d\omega}{2\pi}\{\ln[i\omega+\mu_e-t^2g_{j+1}(i\omega)] -\ln[i\omega+\mu_e-U-t^2g_{j+1}(i\omega)]\}, \tag{34}$$

and $\theta(x)=1$ for $x>0, \theta(x)=0$ for $x<0$. The functions $g_j(i\omega)$ satisfy Eqs. (26) and (27) with $i\omega_n$ replaced by $i\omega$. To solve the zero-temperature equations we proceed as follows. First, we suppose that there exists a period-q solution corresponding to a given sequence $(\alpha_0,\alpha_1,\ldots,\alpha_{q-1})$ where $\alpha_i=0,1$. We will find that noninteger values for α_j are possible only at discrete values of the chemical potentials. We solve the set of equations shown in Eq. (26) for this sequence that yields the functions $g_0,g_1,\ldots,g_{q-1}$. Finally, we compute $X_0(\mu_e,\mu_i),X_1(\mu_e,\mu_i),\ldots,X_{q-1}(\mu_e,\mu_i)$ and then employ Eq. (34) to find the domain of chemical potentials satisfying Eq. (33). Once a phase has been shown to be thermodynamically accessible, we next calculate the interacting density of states $\rho_{int}(\epsilon)=-\Sigma_{j=0}^{q-1}\mathrm{Im}g_j(\epsilon)/(\pi q)$. We will assume in the above analysis that ϵ is measured with respect to the original band structure, so the chemical potential lies at $\epsilon=\mu_e$, not the conventional location at $\epsilon=0$. In this convention, we then have that

$$\rho_e=\int_{-\infty}^{\mu_e}d\epsilon\rho_{int}(\epsilon), \tag{35}$$

and

$$E_{gs}(\rho_e)=\int_{-\infty}^{\mu_e}d\epsilon\epsilon\rho_{int}(\epsilon). \tag{36}$$

The first equation is used to determine the electron chemical potential for a given electron density and the second determines the ground-state energy of the given period-q configuration. To form a restricted phase diagram, we then compare the ground-state energies for a number of different candidate phases, to find which phase is the ground state. Such an analysis does not rigorously establish the true ground state unless all possible candidate states are compared, but it does allow us to prove the existence of higher period phases, if we can find regions of parameter space where the ground state is not the segregated phase, the homogeneous solution, or the period-two phase, which is what we find to be the case below.

The interacting density of states for the homogeneous phase is found from the solution of a simple cubic equation, as first shown by Van Dongen and Leinung.[22] We do not repeat that analysis here. The segregated phase is found by performing a Maxwell construction for the two states corresponding to segregation—the state with $\alpha_0=0$ and the state with $\alpha_0=1$. The former has a density of states equal to the noninteracting density of states, the latter has the noninteracting density of states, but is shifted uniformly upwards in energy by U. We form a mixture of the two ground-state energies, weighted by $1-\rho_i$ for $\alpha_0=0$ and ρ_i for $\alpha_0=1$, with the chemical potential chosen so that the average electron filling is equal to ρ_e. Since the segregated phase at $T=0$ involves the mixture of only the empty and full lattice it is easy to incorporate this phase into our ground-state analysis. Note that in the large-U limit, the full lattice will be unoccupied (if $U>4t^*$), so the electron concentration for the empty lattice becomes $\rho_e/(1-\rho_i)$.

For $q=2$, $\alpha_0=0$, and $\alpha_1=1$, the ground-state equations become

$$g_0(i\omega)=\frac{1}{i\omega+\mu_e-t^{*2}g_1(i\omega)}, \tag{37}$$

$$g_1(i\omega)=\frac{1}{i\omega+\mu_e-U-t^{*2}g_0(i\omega)}, \tag{38}$$

for the Green functions on levels 0 and 1 and

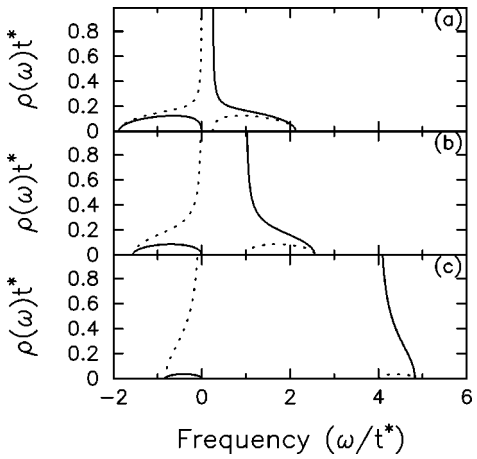

FIG. 1. Interacting density of states at $T=0$ for the period-two charge-density-wave phase at three different values of U: (a) $U=0.25t^*$; (b) $U=t^*$; and (c) $U=4t^*$. The solid line is the density of states for level 0 and the dotted line is for level 1. Note how an interchange of levels and a reflection about $U/2$ is a symmetry operation. As U increases, the density of states becomes two delta functions of weight 0.5 centered at $\omega=0$ and $\omega=U$.

$$X_0(\mu_e,\mu_i)=\mu_i-\int_{-\infty}^{\infty}\frac{d\omega}{2\pi}\{\ln[i\omega+\mu_e-t^{*2}g_1(i\omega)]-\ln[i\omega+\mu_e-U-t^{*2}g_1(i\omega)]\},\tag{39}$$

$$X_1(\mu_e,\mu_i)=\mu_i-\int_{-\infty}^{\infty}\frac{d\omega}{2\pi}\{\ln[i\omega+\mu_e-t^{*2}g_0(i\omega)]-\ln[i\omega+\mu_e-U-t^{*2}g_0(i\omega)]\},\tag{40}$$

with $X_0(\mu_e,\mu_i)<0$ and $X_1(\mu_e,\mu_i)>0$. Equations (37) and (38) reduce to two quadratic polynomials for $g_0(i\omega)$ and $g_1(i\omega)$. The physical solutions are (we set $\zeta=i\omega+\mu_e$)

$$g_0(\omega)=\frac{1}{2t^{*2}}\left[\zeta-U-\sqrt{\frac{\zeta-U}{\zeta}(\zeta^2-U\zeta-4t^{*2})}\right],\tag{41}$$

and

$$g_1(i\omega)=\frac{1}{2t^{*2}}\left[\zeta-\sqrt{\frac{\zeta}{\zeta-U}(\zeta^2-U\zeta-4t^{*2})}\right],\tag{42}$$

where the square root is chosen to lie in the upper half plane for $\omega>0$ and in the lower half plane for $\omega<0$. It is a simple exercise to find regions where the solutions are thermodynamically consistent.

The density of states is nontrivial for these systems and was first examined by Van Dongen.[23] For both levels, there are two bands: the first runs from $\epsilon=(U-\sqrt{U^2+16t^{*2}})/2$ to $\epsilon=0$ and the second from $\epsilon=U$ to $\epsilon=(U+\sqrt{U^2+16t^{*2}})/2$ (note we are plotting these results in an absolute energy scale, so that the chemical potential lies at $\epsilon=\mu_e$). Examples are plotted in Fig. 1 for a few selected values of U. As expected, the density of states for each of the levels (level 0, solid line; level 1, dotted line) has a divergence at one of its band edges, which comes from the pileup of states from the gap formation of the ordered phase. Note that as U becomes large, the bands narrow significantly, and approach delta functions as $U\to\infty$. The filling in the lower band is always equal to 1/2 for all $U>0$. This lack of dependence (of the filling in the lower band) on U turns out to generically not be the case for higher periods. Note also the symmetry between the levels and a reflection plane centered at $U/2$.

We will also be interested in the period-two phase with $\alpha_0=1/3$ and $\alpha_1=1$. This is a phase where μ_i must be adjusted so that the exponent in Eq. (27) vanishes linearly in T as $T\to0$. Since this can only be done for one of the ion densities, the other must be either zero or one. We consider the case of $\alpha_1=1$ here, because we want to examine the ground-state phase diagram for the case $\rho_i=2/3$. The analysis of the density of states is only slightly more complicated than that given above for the $\rho_i=1/2$ case, so we do not provide the details here. The interacting density of states is no longer symmetric though.

We set $q=3$ and $\alpha_0=1,\alpha_1=1,\alpha_2=0$ in the ground-state equations. The cases $\alpha_0=1,\alpha_1=0,\alpha_2=1$, and $\alpha_0=0,\alpha_1=1,\alpha_2=1$ lead to the same result. For the Green functions we now have three coupled equations:

$$g_0(i\omega)=\frac{1}{i\omega+\mu_e-U-t^{*2}g_1(i\omega)},$$

$$g_1(i\omega)=\frac{1}{i\omega+\mu_e-U-t^{*2}g_2(i\omega)},$$

$$g_2(i\omega)=\frac{1}{i\omega+\mu_e-t^{*2}g_0(i\omega)}.\tag{43}$$

Each Green function is again the solution of a quadratic equation that yields (we set $\zeta=i\omega+\mu_e$)

$$g_0(i\omega)=\frac{\zeta[t^{*2}-(\zeta-U)^2]-\sqrt{R(\zeta)}}{2t^{*2}[t^{*2}-(\zeta-U)^2]},$$

$$g_1(i\omega)=\frac{(\zeta-U)[t^{*2}-\zeta(\zeta-U)]-t^{*2}U-\sqrt{R(\zeta)}}{2t^{*2}[t^{*2}-\zeta(\zeta-U)]},$$

$$g_2(i\omega)=\frac{\zeta[t^{*2}-(\zeta-U)^2]-\sqrt{R(\zeta)}}{2t^{*2}[t^{*2}-\zeta(\zeta-U)]},\tag{44}$$

where

$$R(\zeta)=-[2t^{*2}+(U-t^*)\zeta-\zeta^2][2t^{*2}+(U+t^*)\zeta-\zeta^2]\times[t^{*2}-(\zeta-U)^2],\tag{45}$$

and the sign of the square root is chosen to have the correct analyticity properties of g. It is easy to find values of μ_i where $X_0(\mu_e,\mu_i)>0$, $X_1(\mu_e,\mu_i)>0$, and $X_2(\mu_e,\mu_i)<0$, which is the domain where the ion density is equal to 2/3.

The interacting density of states is quite different for the period-three phases. There are three bands

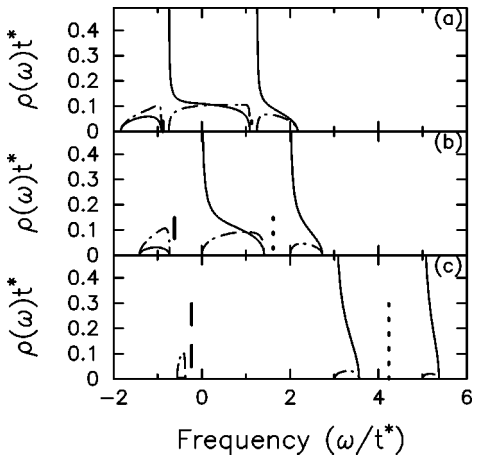

FIG. 2. Interacting density of states for the period-three charge-density-wave phase at three values of U: (a) $U=0.25t^*$; (b) $U=t^*$; and (c) $U=4t^*$. Note how the density of states splits into three bands and two delta functions. The solid line is for level 0, the dotted for level 1, and the dashed for level 2. The densities of states are identical for levels 1 and 2 except for the delta function contributions, which are located between the upper two bands (level 1) or the lower two bands (level 2). The height of the thick lines denotes the weight of the delta functions in the total density of states, which approach 1/3 as $U\rightarrow\infty$.

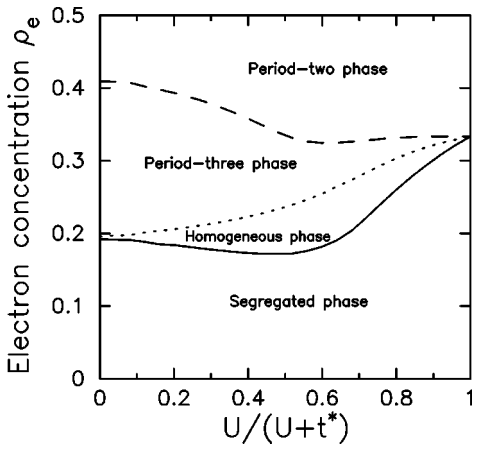

FIG. 3. Restricted ground-state phase diagram for $\rho_i=2/3$. The homogeneous, segregated, period-two (with $\alpha_0=1/3$ and $\alpha_1=1$), and period-three phase (with $\alpha_0=1$, $\alpha_1=1$, and $\alpha_2=0$), are compared to each other and their regions of stability plotted in the figure. Note the wide region of stability of the period-three phase. Note further, that as $U\rightarrow\infty$, the ground state is the segregated phase for $\rho_e+\rho_i<1$, as expected.

located in the following regions: (lower band) $(U-t^*-\sqrt{U^2-2Ut^*+9t^{*2}})/2\leqslant\epsilon\leqslant(U+t^*-\sqrt{U^2+2Ut^*+9t^{*2}})/2$; (middle band) $U-t^*\leqslant\epsilon\leqslant(U-t^*+\sqrt{U^2-2Ut^*+9t^{*2}})/2$; and (upper band) $U+t^*\leqslant\epsilon\leqslant(U+t^*+\sqrt{U^2+2Ut^*+9t^{*2}})/2$. In addition, the Green functions for levels 1 and 2 have poles (i.e., delta-function contributions to the density of states) that have weight $U/\sqrt{U^2+4t^{*2}}$ and are located at $\epsilon=[U+\sqrt{U^2+4t^{*2}}]/2$ ($\epsilon=[U-\sqrt{U^2+4t^{*2}}]/2$) for level 1 (level 2), respectively. The results are plotted in Fig. 2 for some representative cases of U. The functional forms for levels 1 and 2 are identical, except for the delta functions—hence the dotted (level 1) and dashed curves (level 2) overlap except at the delta functions, whose weight is indicated by the height of the thick lines in the figure. Note that as $U\rightarrow\infty$, the delta function contributions become more important for levels 1 and 2, while level 0 generates two delta functions, each of weight 1/2 at $U\pm t^*$. In the period-three case, the pileup of density of states is only seen at level 0—levels 1 and 2 have bounded densities of states except for the delta function contributions. It is interesting to note that in this case, the filling in the lower band plus the lower delta function (all contributions with $\epsilon<0$) ranges from 0.19 550 when $U\rightarrow0$ to 1/3 when $U\rightarrow\infty$. This means that as $T\rightarrow0$ the electron filling for the period-three phase with $\rho_i=2/3$ (with the electronic chemical potential lying in the gap of the electronic density of states) will range from 0.19 550 to 1/3 as a function of U.

We now can construct a restricted ground-state phase diagram, for the case of $\rho_i=2/3$, by comparing the ground-state energies of the homogeneous, segregated, period-two, and period-three phases as a function of ρ_e and U. This phase diagram is plotted in Fig. 3. Notice how the period-three phase is stabilized over a wide range of parameter space in weak coupling, stretching from approximately $\rho_e=0.1955$ to $\rho_e=0.4095$, which narrows as U increases to the point $\rho_e=1/3$ in the strong-coupling limit. The existence of this higher-period ground-state phase proves that higher-period phases exist on the infinite-coordination Bethe lattice, since the period-two, homogeneous, and segregated phases are not the ground state. Since this is a restricted phase diagram we cannot rule out the possibility of higher-period phases possibly being stable and taking over more of the phase diagram, if they were included in the analysis (in fact, we expect them in regions where the homogeneous phase is stable).

In principle, the same computations can be carried out to higher order in q, but the equations become cumbersome, and we leave such an analysis for a future publication.

IV. FINITE-TEMPERATURE ANALYSIS

The finite-temperature analysis for these higher period phases becomes complicated because no simple variant on the iterative schemes for the homogeneous and period-two phases appears to converge for period three and higher, so an alternate computational strategy is needed. We begin by describing how to proceed for the period-two phase and then for the period-three phase. We do not perform any finite-temperature calculations on higher period phases.

We begin with the general equations for the period-two phase at finite temperature:

$$g_0(i\omega_n)=\frac{1-\alpha_0}{i\omega_n+\mu_e-t^{*2}g_1(i\omega_n)}+\frac{\alpha_0}{i\omega_n+\mu_e-U-t^{*2}g_1(i\omega_n)}, \qquad (46)$$

$$g_1(i\omega_n)=\frac{1-\alpha_1}{i\omega_n+\mu_e-t^{*2}g_0(i\omega_n)}+\frac{\alpha_1}{i\omega_n+\mu_e-U-t^{*2}g_0(i\omega_n)},$$

where the fillings on the two levels α_0 and α_1 are unequal in the ordered phase, but are generally not equal to zero or one at finite temperature. Substituting the value for g_1 into the right-hand side of the equation for g_0 in Eq. (46) produces an equation for g_0. This is a quintic polynomial that has four unphysical roots (wrong sign of the imaginary part of g_0) and one physical root, so there is never any ambiguity in determining which root to use. The quintic equation is complicated, but is summarized below, where we use the shorthand notation of $g_0=t^{*2}g_0(i\omega_n)$ and $\zeta=i\omega_n+\mu_e$:

$$\begin{aligned}&g_0[\zeta(\zeta-g_0)(\zeta-U-g_0)-(\zeta-\{1-\alpha_1\}U-g_0)]\\&\quad\times[(\zeta-U)(\zeta-g_0)(\zeta-U-g_0)-(\zeta-\{1-\alpha_1\}U-g_0)]\\&\quad=(\zeta-g_0)(\zeta-U-g_0)[(\zeta-\{1-\alpha_0\}U)(\zeta-g_0)\\&\quad\times(\zeta-U-g_0)-(\zeta-\{1-\alpha_1\}U-g_0)].\end{aligned}\tag{47}$$

The strategy for solving these equations is to first fix the average ion density $\rho_i=(\alpha_0+\alpha_1)/2$ and then to choose a trial difference in ion density $\delta\rho_i=\alpha_0-\alpha_1$. This determines trial values for both α_0 and α_1. Next we solve Eq. (47) for $g_0(i\omega_n)$ by choosing the unique physical root. Then $g_1(i\omega_n)$ is determined from the second equation in Eq. (46). Now we calculate the chemical potential for the ions using the infinite product in Eq. (27) with $j=0$ and we call that chemical potential μ_{i0}. We perform the same calculation with $j=1$ to determine μ_{i1}. In general, these two chemical potentials will not be equal because $\delta\rho_i$ was not chosen to be equal to the correct value for the thermodynamic state at the given temperature, so we adjust $\delta\rho_i$ until we find a solution where the two ''chemical potentials'' for the levels 0 and 1 are equal. This then is the solution to the thermodynamic problem. Note that in the ordered phase there are always two nontrivial solutions with $\delta\rho_i\geqslant 0$: (i) the first has $\delta\rho_i=0$ and corresponds to the homogeneous phase and (ii) the second has $\delta\rho_i>0$ and corresponds to the ordered phase. We never found any multiple solutions within the ordered phase, and this algorithm was generically quite stable.

We find that this solution method is relatively quick and it works better than the iterative techniques when one is close to the phase transition, since one is controlling the value of the order parameter $\delta\rho_i$ externally and not relying on developing it in an iterative algorithm (which can become subject to critical slowing down). Comparing solutions for T_c to the period-two phase with more conventional techniques based either on calculating the susceptibility in the homogeneous phase or calculating the ordered phase using an iterative scheme, all agree to five decimal places, so we have confidence that this technique works well for determining solutions to the coupled ordered-phase equations.

We use the same procedure to solve for the ordered phases of the period-three solutions. The equations for the Green functions are

$$\begin{aligned}g_0(i\omega_n)&=\frac{1-\alpha_0}{i\omega_n+\mu_e-t^{*2}g_1(i\omega_n)}+\frac{\alpha_0}{i\omega_n+\mu_e-U-t^{*2}g_1(i\omega_n)},\\g_1(i\omega_n)&=\frac{1-\alpha_1}{i\omega_n+\mu_e-t^{*2}g_2(i\omega_n)}+\frac{\alpha_1}{i\omega_n+\mu_e-U-t^{*2}g_2(i\omega_n)},\\g_2(i\omega_n)&=\frac{1-\alpha_2}{i\omega_n+\mu_e-t^{*2}g_0(i\omega_n)}+\frac{\alpha_2}{i\omega_n+\mu_e-U-t^{*2}g_0(i\omega_n)}.\end{aligned}\tag{48}$$

Substituting the equation for g_2 into the equation for g_1 and then substituting the resultant relation for g_1 into the equation for g_0 produces a single equation for g_0 that depends on the ion concentrations in each level. It is an order-nine polynomial that, once again, shows only one physical solution for the Green function. The equation is cumbersome and the algebra is straightforward, so we will not display the equation here.

We adopt the same algorithm for solving this problem. First, we fix the average ion filling $\rho_i=(\alpha_0+\alpha_1+\alpha_2)/3$. Then we choose α_0 to be equal to a fixed value, and we choose a trial value for α_1, which also determines the trial value for α_2. We adjust α_1 so that the ''chemical potentials'' for the ions determined by Eq. (27) with $j=0$ and $j=1$ are equal. We then calculate the ''chemical potential'' for level 2 by using Eq. (27) with $j=2$. If this value is not equal to the chemical potential determined for levels 0 and 1, then we adjust α_0 and start the procedure all over again. It is quite challenging to find the regions of parameter space that yield nontrivial solutions and we are generically guided by the solutions found at $T=0$ as our starting point, we then slowly raise the temperature to see how those solutions evolve. Our strategy involves calculating these results on a grid of points for α_0 and α_1 until we reach a region where a solution to the equations is possible, and then we use one-dimensional root-finders to zero in on the correct values of the ion fillings. Calculations are much easier to perform at fixed values of the electronic chemical potential, rather than adjusting that chemical potential as a function of temperature to keep the electron filling constant. We illustrate solutions in both cases of fixed ρ_e and fixed μ_e.

Once the fillings on each level and the chemical potentials have been determined, we can make the analytic continuation of the Green-function equations (26) by simply taking $i\omega_n\rightarrow\omega+i\delta$. This produces a series of equations on the real

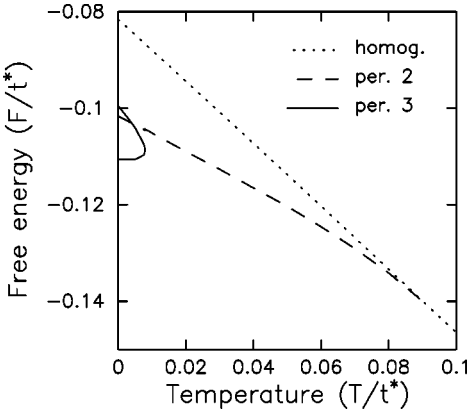

FIG. 4. Free energy for candidate low-energy phases at $U=3t^*$, $\rho_i=2/3$, and $\mu_e=0.84\,861$ (corresponding to $\rho_e\approx 0.332$). The solid curve is the period-three solution, the dashed is the period-two, and the dotted is the homogeneous phase. Note how the period-two phase intersects the homogeneous phase curve with the same slope, as expected for a second-order phase transition, and how the period-three phase must have a phase transition to a higher period phase at an intermediate temperature (most likely first order) because the free energy cannot be discontinuous at T_c and the free energy is not multivalued.

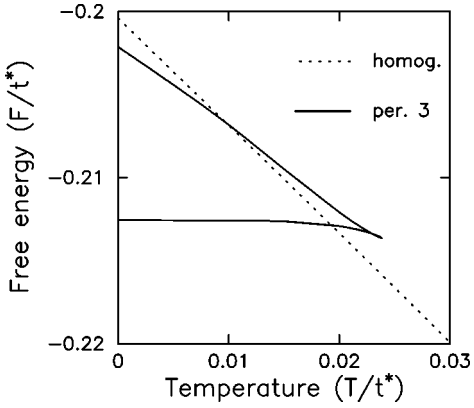

FIG. 5. Free-energy plot for the period-three and homogeneous phases for $U=t^*$, $\rho_i=2/3$, and $\rho_e=0.26\,698$. Note how the phase transition is clearly first-order here. The period-two phase is never stable, because the electron density is too close to zero. There is no need for additional higher period phases to be stable here, but we cannot rule out that possibility.

axis that can also be solved directly (in essence, we simply use the same polynomial equation, but now evaluated on the real axis). This allows us to determine the Green functions on the real axis, and therefore, the average interacting density of states

$$\rho_{int}(\epsilon)=-\frac{1}{q\pi}\mathrm{Im}\sum_{j=0}^{q-1} g_j(\epsilon). \tag{49}$$

Once the density of states has been determined, then we can directly calculate the free energy, which assumes the following generalization of the original Falicov-Kimball form:[3,24]

$$F=\mu_e\rho_e+T\int_{-\infty}^{\infty} d\epsilon\rho_{int}(\epsilon)\ln\frac{e^{\beta(\epsilon-\mu_e)}}{1+e^{\beta(\epsilon-\mu_e)}} + \frac{T}{q}\sum_{j=0}^{q-1}[\alpha_j\ln\alpha_j+(1-\alpha_j)\ln(1-\alpha_j)]. \tag{50}$$

We find when we calculate the ordered period-three phases, they are stable only for relatively low temperatures. Hence, the ion density on each of the levels changes only slightly from the values at $T=0$. Hence, the density of states is only slightly modified as a function of temperature. We do not plot the temperature dependence here because it is so mild. Instead, we plot the free energy as a function of temperature. Figure 4 is calculated at a constant chemical potential ($\mu_e=0.84\,861, \rho_e\approx 0.332$), chosen to lie in the region where the period-three phase is stable, at a coupling strength $U=3$. This value was chosen because it is large enough that the system behaves as it does in the strong-coupling limit, but is small enough that the transition temperature does not become too small. The figure shows the homogeneous free energy, the period-two free energy, and the period-three free energy. There are two period-three solutions, but only one of them is thermodynamically stable at any given temperature. Note how the period-two free energy matches the slope of the homogeneous free energy at the point that they touch. This is characteristic of a second-order phase transition. On the other hand, the stable branch of the period-three free energy intersects neither the period-two nor the homogeneous phases before it curves back on itself and joins the unstable branch. This implies that there must be another higher period thermodynamically stable phase that is present at an intermediate range of temperatures, and has a phase transition (most likely) to the period-two phase before becoming homogeneous at the highest temperature. Clearly, the phase diagram in this region of parameter space is quite complicated. We have not determined which alternate phases are stable in this intermediate temperature range.

Our second example is at a weaker value of the coupling strength, $U=1$, which is presented in Fig. 5. In this case, the period-two phase is never stable, because the electron filling is too low to sustain the chessboard phase (note the distance to the period-two phase in the ground-state phase diagram of Fig. 3). Instead, there is a direct phase transition from the period-three phase to the homogeneous phase. This phase transition is also first order, as can be seen from the mismatch of the slopes of the free energies at the point where they cross. Note that this calculation was performed at a constant electron filling of $\rho_e=0.26\,698$.

V. CONCLUSION

We have used two techniques to show the existence of higher period phases on the infinite-coordination Bethe lattice. The first was a restricted phase diagram analysis at $T=0$, which showed that higher period phases must exist on the Bethe lattice. The second was an examination of the system at finite temperature, where we were able to see that generically, the phase transition to the period-three phase is first order and that higher period phases must be stabilized at

strong coupling and intermediate temperatures, in order for the system to have the proper thermodynamics. This work has discussed a long-standing controversy about whether or not these higher period phases can exist on the Bethe lattice. We have left open the question of a more complete study of these systems, to see if the behavior in the one-dimensional lattice is also seen here, such as a Farey-tree structure. It is possible that the techniques we developed here could also be applied to the hypercubic lattice, but the results are likely to be much different there, as the hypercubic lattice can sustain second-order phase transitions to incommensurate and higher period phases.

ACKNOWLEDGMENTS

J.K.F. acknowledges the support of the Office of Naval Research under Grant No. N00014-99-1-0328. J.K.F. also acknowledges the hospitality of the EPFL where this work was completed.

APPENDIX: LARGE COORDINATION-NUMBER LIMIT OF THE GREEN FUNCTION

Here we show that the difference between $G^*_{zz}(i\omega_n)$ and $G_{zz}(i\omega_n)$ in Eq. (23) is $O(Z^{-1})$ and compute the first correction. We rewrite the local effective action (16) associated to site z in the following form:

$$S^{\Lambda}_{n,eff}(w_z)=S^{\Lambda(y;z)}_{n,eff}(w_z)+\frac{t^{*2}_{zy}}{Z}G^{\Lambda(z;y)}_{yy}(i\omega_n)\overline{\psi}_z(i\omega_n)\psi_z(i\omega_n). \tag{A1}$$

For Eq. (17) we have to order Z^{-1}

$$Z_{\Lambda,eff}=Z_{\Lambda(y,z),eff}\left[1-\frac{t^{*2}_{zy}}{Z}\sum_{n=-\infty}^{\infty}G^{\Lambda(z;y)}_{yy}(i\omega_n)\times\langle\overline{\psi}_z(i\omega_n)\psi_z(i\omega_n)\rangle^{\Lambda(y,z)}_{eff}\right], \tag{A2}$$

where $\langle\overline{\psi}_z(i\omega_n)\psi_z(i\omega_n)\rangle^{\Lambda(y,z)}_{eff}$ is defined as in Eq. (15) but with $S^{\Lambda(y;z)}_{n,eff}(w_z)$ replacing $S^{\Lambda}_{n,eff}(w_y)$. Therefore, to leading order

$$Z^{-1}_{\Lambda,eff}=Z^{-1}_{\Lambda(y,z),eff}\left[1-\frac{t^{*2}_{zy}}{Z}\times\sum_{n=-\infty}^{\infty}G^{\Lambda(z;y)}_{yy}(i\omega_n)G^{\Lambda(y;z)}_{zz}(i\omega_n)\right]. \tag{A3}$$

From Eqs. (15), (A1), and (A3) we get

$$G^{\Lambda}_{zz}(i\omega_n)=\left[1-\frac{t^{*2}_{zy}}{Z}\sum_{n=-\infty}^{\infty}G^{\Lambda(z;y)}_{yy}(i\omega_n)G^{\Lambda(y;z)}_{zz}(i\omega_n)\right]\times\left[\langle\psi_z(i\omega_n)\overline{\psi}_z(i\omega_n)\rangle^{\Lambda(y,z)}_{eff}-\frac{t^{*2}_{zy}}{Z}\times\sum_{m=-\infty}^{\infty}G^{\Lambda(z;y)}_{yy}(i\omega_m)\times\langle\overline{\psi}_z(i\omega_m)\psi_z(i\omega_m)\psi_z(i\omega_n)\overline{\psi}_z(i\omega_n)\rangle^{\Lambda(y,z)}_{eff}\right], \tag{A4}$$

so that to leading order we find

$$G^{\Lambda}_{zz}(i\omega_n)=G^{\Lambda(y,z)}_{zz}(i\omega_n)-\frac{t^{*2}_{zy}}{Z}[G^{\Lambda(y,z)}_{zz}(i\omega_n)]^2G^{\Lambda(z,y)}_{yy}(i\omega_n). \tag{A5}$$

Assuming that the thermodynamic limits exist, we find to lowest order

$$G^*_{zz}(i\omega_n)=G_{zz}(i\omega_n)+\frac{t^{*2}}{Z}[G_{zz}(i\omega_n)]^2G_{yy}(i\omega_n), \tag{A6}$$

which justifies the procedure outlined in the main text.

[1] W. Metzner and D. Vollhardt, Phys. Rev. Lett. **62**, 324 (1989).
[2] A. Georges, G. Kotliar, W. Krauth, and M. J. Rozenberg, Rev. Mod. Phys. **68**, 13 (1996).
[3] L. M. Falicov and J. C. Kimball, Phys. Rev. Lett. **22**, 997 (1969); R. Ramirez, L. M. Falicov, and J. C. Kimball, Phys. Rev. B **2**, 3383 (1970).
[4] D. I. Khomskii, Usp. Fiz. Nauk. **129**, 443 (1979) [Sov. Phys. Usp. **22**, 879 (1979)]; D. I. Khomskii, in *Quantum Theory of Solids*, edited by I. M. Lifshits (Mir, Moscow, 1982).
[5] A. Sakurai and P. Schottman, Solid State Commun. **27**, 991 (1971).
[6] T. Kennedy and E. H. Lieb, Physica A **138**, 320 (1986).
[7] N. Macris and Ch. Gruber, Helv. Phys. Acta **69**, 850 (1996); K. Michielsen, Int. J. Mod. Phys. B **7**, 2571 (1993).
[8] P. Lemberger, J. Phys. A **25**, 715 (1992).
[9] Ch. Gruber, D. Ueltschi, and J. Jedrzejewski, J. Stat. Phys. **76**, 125 (1994).
[10] Ch. Gruber, N. Macris, A. Messager, and D. Uetschi, J. Stat. Phys. **86**, 57 (1997).
[11] J. K. Freericks and L. M. Falicov, Phys. Rev. B **41**, 2163 (1990).
[12] J. K. Freericks, Ch. Gruber, and N. Macris, Phys. Rev. B **53**, 16 189 (1996).
[13] M. Barma and V. Subrahmanyan, Phase Transitions **16**, 307 (1996).
[14] Ch. Gruber, J. Jedrzejewski, and P. Lemberger, J. Stat. Phys. **66**, 913 (1996).
[15] T. Kennedy, Rev. Math. Phys. **6**, 901 (1994).
[16] T. Kennedy, J. Stat. Phys. **91**, 829 (1998).
[17] G. I. Watson, Physica A **246**, 253 (1997).
[18] U. Brandt and C. Mielsch, Z. Phys. B: Condens. Matter **75**, 365 (1989); **79**, 295 (1990); **82**, 37 (1991).

[19] J. K. Freericks, Phys. Rev. B **47**, 9263 (1993).
[20] J. K. Freericks, Ch. Gruber, and N. Macris, Phys. Rev. B **60**, 1617 (1999).
[21] J. K. Freericks and R. Lemanski, Phys. Rev. B **61**, 13 438 (2000).
[22] P. G. J. Van Dongen and C. Leinung, Ann. Phys. (Leipzig) **6**, 45 (1997).
[23] P. G. J. Van Dongen, Phys. Rev. B **45**, 2267 (1992).
[24] W. Chung and J. K. Freericks, Phys. Rev. B **57**, 11 955 (1998).